Management and Production Engineering Review
Volume 17 • Number 2 • June 2026 • pp. 1–13
DOI: 10.24425/mper.2026.1326

An Approach to Design a Prototype of Lattice Structures: a Preliminary Study

Wiktoria WOJNICZ, Keyru Salia SURAJ, Klaudia PIWKO, Klaudia HIRSCH

Faculty of Mechanical Engineering and Ship Technology, Gdansk University of Technology, Poland

Received: 19 November 2025
Accepted: 15 March 2026

Abstract
This paper investigates the mechanical response of lattice cells based on numerical models and 3D printed specimens. Considering the growing interest in the application of lattice structures in engineering and biomedical research, the design of lattice structures is becoming one of the key areas of modern materials engineering. The goal of this study is to develop author lattice cells that can be used in porous implants maintaining external compression loading. In the scope of this study, four author lattice cells were designed and produced from Acrylonitrile Butadiene Styrene (ABS) material using Zortrax M200 and Bambu Lab A1 3D printers (fused deposition modelling (FDM) technology) without using any supporting materials. A uniaxial compression test was performed using Zwick/Roell Z020. A numerical analysis of proposed lattice cells was conducted in FEBio and Abaqus. Young's moduli of all tested lattice cells were assessed from experimental and numerical data along with relative errors. The Young's modulus was identified in the range: the smallest was 14.24 MPa (experimental) with 27.00/25.00 MPa (numerical) and the largest was 571.33 MPa (experimental) with 611.69/641.27 MPa (numerical). This study presents a validated numerical-experimental protocol that can be applied to produce FDM-printed lattice cell structures through closed iteration approach by considering given requirements along with technological limitations of FDM printings (manufacturing-induced flaws, staircase effects, and anisotropic polymer layer-bonding effects). Presented findings reveal that the designed topologies of lattice cells depend on the resolution of used 3D printers, however proposed numerical-experimental protocol offers a low-cost promising pathway for the early-stage design of patient-specific bone tissue implants.

Keywords
lattice cell, Uniaxial compression, FDM.

Introduction

Cellular structures are identified in many living organisms, wood, natural bones, sponges, and diatoms (Gibson, 2003; Theriot & Herbarium, 1992). Geometrical configurations of cellular structures include open-cell and closed-cell foams, honeycombs, and lattice structures (Gibson & Ashby, 1982; Gibson & Ashby, 1997). Foam cell shapes are randomly shaped, and their walls are characterized by random orientations in space. Honeycombs are considered as structures with regular geometry and identical cells that can form hexagonal prisms (Tang & Zhao, 2016), chiral honeycomb, and auxetic structures (Qi et al., 2016). Lattice structures are characterized by regular geometrical arrangements that can be considered as patterns with spatially arranged cells composed of defined edges and surfaces. These patterns can be homogenous or heterogeneous. Considering mechanical properties, lattice structures are characterized by higher properties with respect to the properties of foams and honeycombs (Yang et al., 2012). For example, properly designed lattice structures can exhibit greater compressive strength and shear strength compared to the foams and honeycombs (Dong et al., 2017).

Considering the growing interest in the application of lattice structures in engineering area (energy absorption (Evans et al., 2010), energy storage (Karageorgiou & Kaplan, 2005; Narita et al., 2021), structural components and supports (Wadley, 2005; Stampfl et al., 2011; Chibinyani et al., 2025) and biomedical research (biomaterials (Karageorgiou & Kaplan, 2005; Hutmacher, 2000), implants (Stampfl et al., 2011; Yang et al., 2013; Wojnicz et al., 2021), the design of lattice structures

***Corresponding author**: Wiktoria Wojnicz – Faculty of Mechanical Engineering and Ship Technology, Gdansk University of Technology, phone: +48 58 347-13-24, e-mail: wiktoria.wojnicz@pg.edu.pl*

© 2026 The Author(s). This is an open access article under the CC BY license (http://creativecommons.org/licenses/by/4.0/)

is becoming one of the key areas of modern materials engineering. Furthermore, the ability to customize the geometry of individual lattice structures allows for precise shaping to obtain lightweight and durable structures with proper mechanical properties (Han & Lu, 2018; Pan et al., 2020; Fassi & Aniyou, 2023). For example, a design of bone porous implant should consider the fact that stiffness of the artificial bone (or its fragment) must be precisely tuned to the stiffness of adjacent natural bone to avoid an occurrence of stress shielding phenomenon (Wojnicz et al., 2021; Prochor et al., 2020). Additionally, one should remember that natural bone is an anisotropic structure whose mechanical properties are gradually varying and dependent on the direction of the applied load (Geraets et al., 2008). That is why developing artificial bone should be a structure with controlled anisotropy (Gurtner & Durand, 2014; Xu et al., 2016).

Advances in Additive Manufacturing (AM) technologies now enable the production of lattice structures that cannot be produced by using conventional technologies (Giannitelli et al., 2014). However, there are still technological limitations that are dependent on the technology used for 3D printing. To meet given requirements referring to the designing of lattice structures, one should select appropriate geometric parameters, such as cell size, wall thickness along with wall shape, and spatial arrangement (Dong et al., 2020). These parameters are closely related to the technological limitations of 3D printing, such as minimum wall thickness or the stability of unsupported fragments (Stanković et al., 2015; Stanković et al., 2017). The other important parameter in a lattice structure used to measure the degree of porosity is relative density, which is the ratio of the volume of the lattice structure to the volume of solid equivalent of this structure (Wojnicz et al., 2021).

The Fused Deposition Modeling (FDM) is an AM method that allows producing lattice structures with low cost and material versatility (Fang et al., 2020). However, the disadvantages of the FDM method are technical limitations related to the scale of 3D printing, occurrence of unwanted porosity, and material anisotropy (Garzon-Hernandez et al., 2020).

Evidence related to assessment of mechanical properties of FDM printed samples illustrates growing emphasis on experimental-based, parameter-dependent, and geometry-aware approaches to understand non-linear mechanical FDM behavior, for example Dimitrellou et al. (2025) demonstrated the suitability of FDM printed samples for the chosen areas of practical application by developing a multi-criteria decision-making strategy to evaluate key material attributes across a wide range of thermoplastic polymers. Kaur et al. (2022) showed that mechanical properties of FDM printed specimens from Acrylonitrile Butadiene Styrene (ABS) are dependent on layer height, build orientation, printing speed, air gap, infill density, infill pattern, raster angle, raster width, and bed temperature. Furthermore Haque et al. (2025), emphasized that a nozzle diameter of the FDM printer significantly influences mechanical properties of printed specimens manufactured from chosen polymers including ABS. Also (Szemeti & Ramanujan, 2022) pointed out that geometry of the printed FDM sample should be carefully designed based on geometry-aware material modeling. A paper Shi et al. (2024) presents results of tensile strength prediction for Polylactic Acid (PLA) printed samples and deduces that increased raster angle can improve load transfer along filament paths. Moreover, Ali et al. (2024) showed that polymer blending could enhance mechanical properties of FDM printed samples.

Numerical analysis of designed lattice cells (their assembly) can be performed using the Finite Element Method (FEM) that possesses a powerful ability to predict phenomena and to perform a parametric investigation of the designed numerical model. However, this numerical model should involve a proper material model implementation, especially for a designed lattice cell that is supposed to be produced by using the FDM method. This consideration is very important since each FDM printed structure is produced by layering filaments.

In this study, we assume that a lattice cell is to be the smallest repeating unit of a lattice structure (assembly). In this paper, we present the results of numerical analysis and experimental testing of four author lattice cells that were subjected to static uniaxial compression loading.

Research Problem

The inspiration of this study is to design lattice structures that could be used as porous implants or artificial bones that are able to maintain external loading and possess mechanical properties close to the mechanical properties of the skeletal tissue. The motivation to deal with porous structures is evidence demonstrating the advantages of lattice structures over their solid-state counterparts (Tang et al., 2025).

The purpose of this study is to design author lattice cells by using regular shapes (type A) and Triply Periodic Minimal Surfaces (TPMS) (type B) along with meeting a requirement that these new lattice cells can be produced by the FDM method without applying any supporting materials. The reason for this requirement is our observation that detaching supporting materials from the printed specimen can damage its surface. In this preliminary study, we describe two models of type A along with two models of type B and present results referring to assessment of mechanical properties in the linear elastic-range of material behavior related to static uniaxial compression loading obtained from experimental testing and numerical analysis.

The scope of this study covers design of new lattice cells, their manufacturing using FDM, numerical analysis (FEBio and Abaqus), validation and analysis of results. The accurate and reliable prediction of the mechanical behavior of proposed lattice cells under various loading conditions is critical for advancing their development.

FEA software, such as the open-source FEBio and the commercial Abaqus, are widely used to model mechanical behavior of designed lattice cells. However, in literature there is lack of evidence related to the rigorous comparative analysis assessing the correctness of numerical results obtained from application of these two software packages, especially when their results are directly benchmarked against experimental data obtained from testing.

Considering literature referring to lattice structures manufacturing and numerical analysis along with the previous experience described in Wojnicz et al. (2021), the authors developed new 3D geometrical models of lattice cells described in Table 1. These models were created and updated by considering technical limitations of FDM printers.

Table 1
General specifications of the lattice cells

Name	Type	Relative Density (ρr)
Body Centered Prismatic (BCP)	Strut-based	8.77%
Cube with Spherical Void (CSV)	Surface-based	30.27%
Gyroid Sheet (GSH)	Surface-based	32.31%
Gyroid Skeletal (GSK)	Surface-based	66.17%

The authors performed numerical analyses of the proposed lattice cells in FEBio and Abaqus software. For experimental testing, the physical models (specimens) of the proposed lattice cells were produced from ABS material. This material was chosen since its mechanical properties are close to the ones of bone tissue in the linear elastic range of material behavior (Wojnicz et al., 2021; Chatzigeorgiou et al., 2022). Later, the specimens of presented cells were tested by conducting mechanical tests, and these experimental results were used for validation of numerical models of lattice cells.

The models of BCP (Fig. 1a) and CSV (Fig. 1b) have been designed in the Autodesk Inventor Professional modelling software. The BCP lattice cell is a strut-based lattice cell with a strut diameter of 1.2 mm and angle of 45°. The CSV lattice cell is constructed by creating a centrically placed spherical void with 11.2 mm diameter in the cube with 10 mm edge. The GSH (Fig. 1c) and GSK (Fig. 1d) models have been designed using lattice KARAK software (Kamal-k-s, 2025) with a level set value of 0.5. This value determines the relation between shell thickness and relative density of TPMS structures (Chatzigeorgiou et al., 2022). The mathematical representation of Gyroids is given by Equation (1):

$$f(x, y, z) = \cos(x) \cdot \sin(y) + \cos(y) \cdot \sin(z) + \cos(z) \cdot \sin(x) = t \quad (1)$$

The Gyroid skeletal is defined by ($f(x, y, z) < t$ or $f(x, y, z) \geq t$) and the Gyroid sheet is defined by ($-t \leq f(x, y, z) \leq t$) (Al-Ketan et al., 2020).

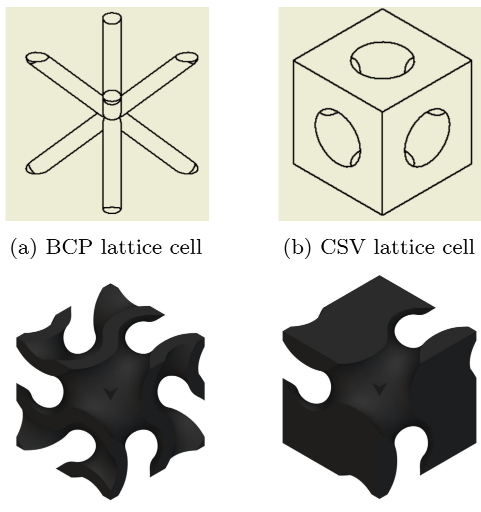

(a) BCP lattice cell (b) CSV lattice cell
(c) GSH lattice cell (d) GSK lattice cell

Fig. 1. 3D models of the lattice cells

It is worth noticing that our approach related to the design of surface-based structures considered following evidence referring to the trends of research focusing on mechanical behavior prediction of TPMS structures. A study Mishra & Kumar (2023) demonstrated the characteristic nonlinear mechanical response of TPMS lattices by considering three following stages (elastic region, topology-dependent plateau and densification stage) and concluded that deformation patterns is sensitive to strain-rate. Furthermore Mahmud et al. (2024), established that TPMS architectures (continuous surfaces) possess significantly higher energy-absorption capacity than conventional strut-based lattices. Ansari et al. (2024) further revealed rate-dependent hardening along with variations in plateau smoothness and concluded that nonlinear response of TPMS structures is governed jointly by material behavior and loading conditions. Moreover, a paper Li et al. (2025) examined hybrid sheet-based TPMS systems and demonstrated that hybridizing different TPMS topologies produces stronger strain-hardening effects and substantially greater energy absorption than any individual TPMS structure. Sun et. al. (2025) presented results of influence of pore shape, porosity, pore diameter, and curvature on the mechanical properties of TPMS structures.

To perform numerical analysis, mechanical properties of a material model were defined in the following way. Ten cubic base specimens with 100% fill density were manufactured from ABS material using two FDM 3D printers: Zortrax M200 and Bambu Lab A1. These specimens were tested using the Zwick/Roell Z020 testing machine with a static uniaxial loading being applied in the printing direction, i.e., perpendicular to the layer of printed filaments. The Young's moduli were determined from the test results: 1100 MPa (Bambu ABS) and 850 MPa (Z-ABS).

Finite element analysis was performed in both FEBio and Abaqus using a linear-elastic material model, with properties defined by the Young's Modulus of the FDM-printed ABS (Table 2 & Table 3) and a Poisson's Ratio of 0.35 (Wojnicz et al., 2021). To obtain numerically convergent and high accuracy results, we adopted different meshes and chose the optimum one for each lattice cell model. The Boundary conditions (BCs) were imposed in the following way: 1) in each numerical model (Figs. 2–5) the base surface was constrained along the Y-th axis while permitting translation in the XZ-th plane; 2) at this base surface we fully fixed a central node in GSH and GSK model, a node on the inner circle in CSV model, and a node on one of the four legs of BCP model. Uniaxial compression loading was implemented in each lattice cell model through kinematic loading imposed on the top surface with a prescribed downward (Negative Y direction) displacement equaled 0.1 mm (Figs. 2–5).

Table 2
Specifications of numerical models of lattice cells created in FEBio

Name of lattice cell	**Overall Dimension (mm)**	**Type of Elements**	**Number of Elements**	**Number of Nodes**	**E (MPa)**
BCP	8.27×8.27×10.00	Quadratic (Tet10)	62 362	103 557	850
CSV	10.00×10.00×10.00	Quadratic (Tet10)	363 711	78 681	1 100
GSH	10.00×10.00×10.00	Quadratic (Tet10)	126 853	212 791	850
GSK	10.00×10.00×10.00	Linear (Tet4)	1 306 955	246 274	1 100

Table 3
Specifications of numerical models of lattice cells created in Abaqus

Name of lattice cell	**Overall Dimension (mm)**	**Type of Elements**	**Number of Elements**	**Number of Nodes**	**E (MPa)**
BCP	8.27×8.27×10.00	Quadratic (C3D10)	44 629	69 276	850
CSV	10.00×10.00×10.00	Quadratic (C3D10)	184 381	285 314	1 100
GSH	10.00×10.00×10.00	Quadratic (C3D10)	104 278	159 515	850
GSK	10.00×10.00×10.00	Quadratic (C3D10)	239 712	344 474	1 100

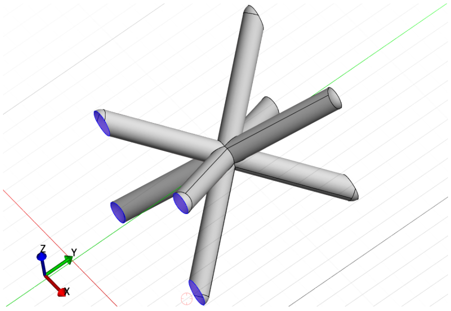

(a) FEBio

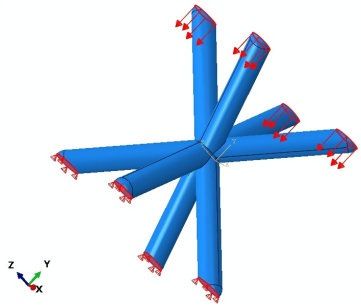

(b) Abaqus

Fig. 2. BCs for BCP lattice cell

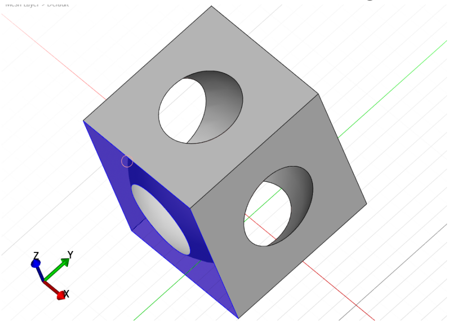

(a) FEBio

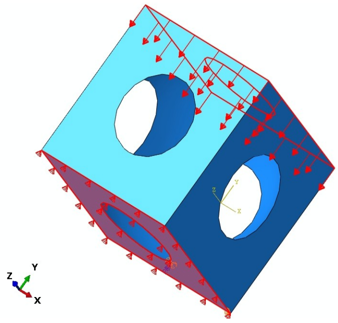

(b) Abaqus

Fig. 3. BCs for CSV lattice cell

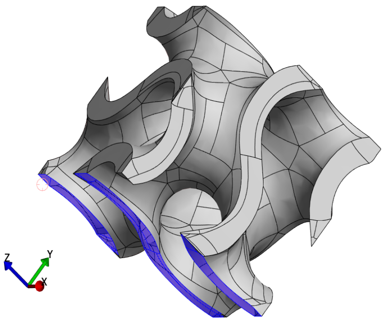

(a) FEBio

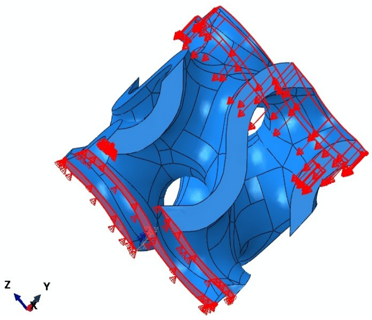

(b) Abaqus

Fig. 4. BCs for GSH lattice cell

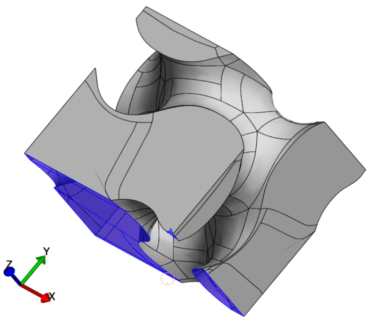

(a) FEBio

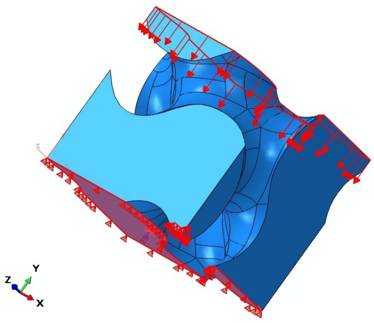

(b) Abaqus

Fig. 5. BCs for GSK lattice cell

To conduct an experimental testing, we printed five specimens of each lattice cell (Fig. 6a (BCP), Fig. 6b (CSV), Fig. 6c (GSH), and Fig. 6d (GSK)). The geometrical parameters of each lattice cell are given in Table 4. Static uniaxial compression tests were conducted under kinematic loading of 10 mm/minute by installing each lattice cell specimen in the center of two parallel and frictionless plates of the Zwick/Roell Z020 testing machine with initial force equaled 10 N.

Table 4
Geometrical parameters of printed samples of lattice cells

Name	Overall Dimension (mm)
BCP lattice cell	15.00×15.00×18.17
CSV lattice cell	20.00×20.00×20.00
GSH lattice cell	15.00×15.00×15.00
GSK lattice cell	20.00×20.00×20.00

Results

Numerical Analysis Results

The results of numerical analysis of each lattice cell are presented in the form of distribution maps visualizing normal stress calculated along the Y axis (the direction of static uniaxial compression loading): 1) FEBio software; (Fig. 7a (BCP), Fig. 8a (CSV), Fig. 9a (GSH) and Fig. 10a (GSK)) and 2) Abaqus software; (Fig. 7b (BCP), Fig. 8b (CSV), Fig. 9b (GSH) and Fig. 10b (GSK)).

Experimental Testing Results

Results of experimental stress-strain curves of all specimens of each lattice cell are presented in Fig. 11a) BCP, Fig. 11b) CSV, Fig. 11c) GSH and Fig. 11d), GSK.

Young's Modulus Results

The results of Young's Moduli for all four lattice cells are calculated from the data obtained from numerical analyses in FEBio and Abaqus along with experimental testing (Table 5 and Fig. 12).

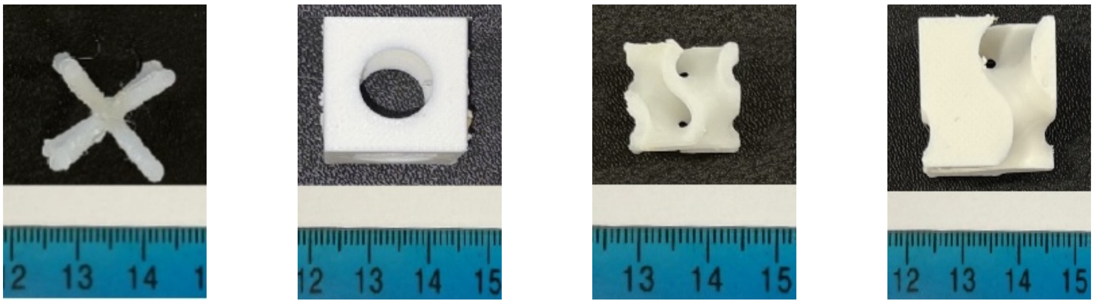

(a) BCP lattice cell (b) CSV lattice cell (c) GSH lattice cell (d) GSK lattice cell

Fig. 6. Sample specimen of all tested lattice cells

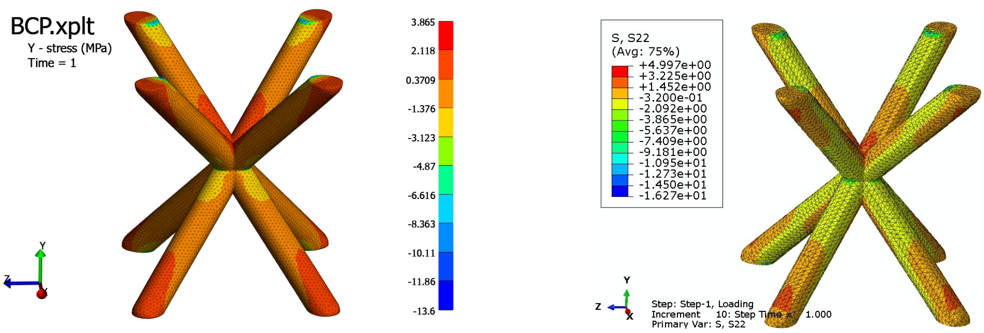

(a) FEBio (b) Abaqus

Fig. 7. Normal stress results of BCP Lattice cell

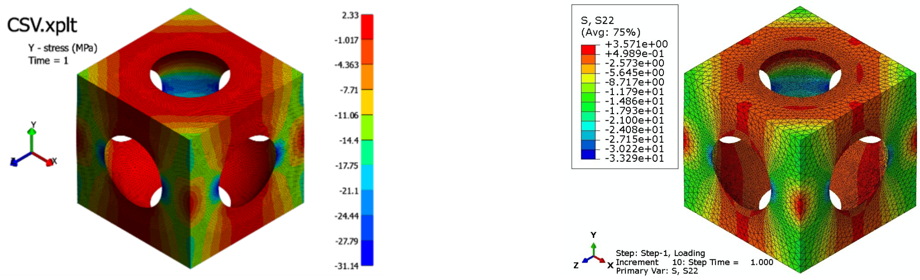

(a) FEBio (b) Abaqus

Fig. 8. Normal stress results of CSV lattice cell

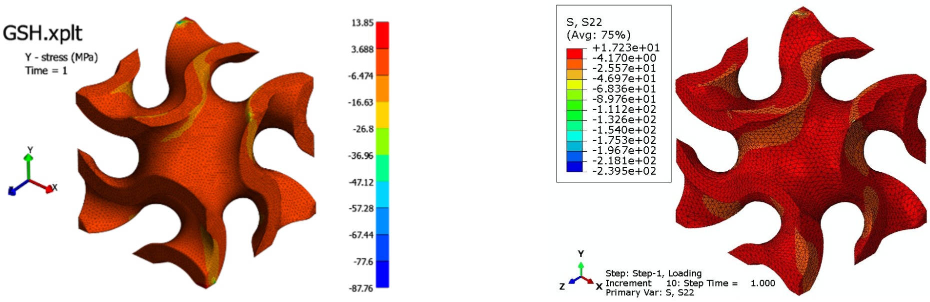

(a) FEBio (b) Abaqus

Fig. 9. Normal stress results of GSH lattice cell

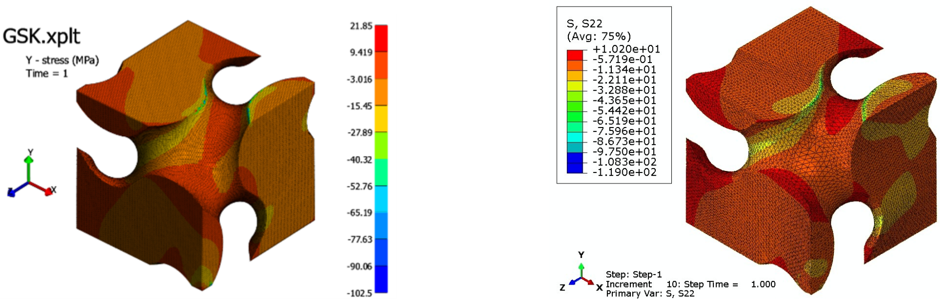

(a) FEBio (b) Abaqus

Fig. 10. Normal stress results of GSK lattice cell

Table 5
Numerical and Experimental Results of lattice cells and their specimens

Name of lattice cell	**Young's Modulus (MPa)**			**Relative Error with respect to the mean of experimental result (%)**	
	FEBio	Abaqus	Experimental (mean ±SD)	FEBio Error	Abaqus Error
BCP	27.00	25.00	14.24 ±1.10	47.26	45.23
CSV	456.90	464.92	532.97 ±18.80	16.65	14.64
GSH	238.22	231.54	302.08 ±10.80	30.40	30.46
GSK	611.69	641.27	571.33 ±48.99	6.60	10.91

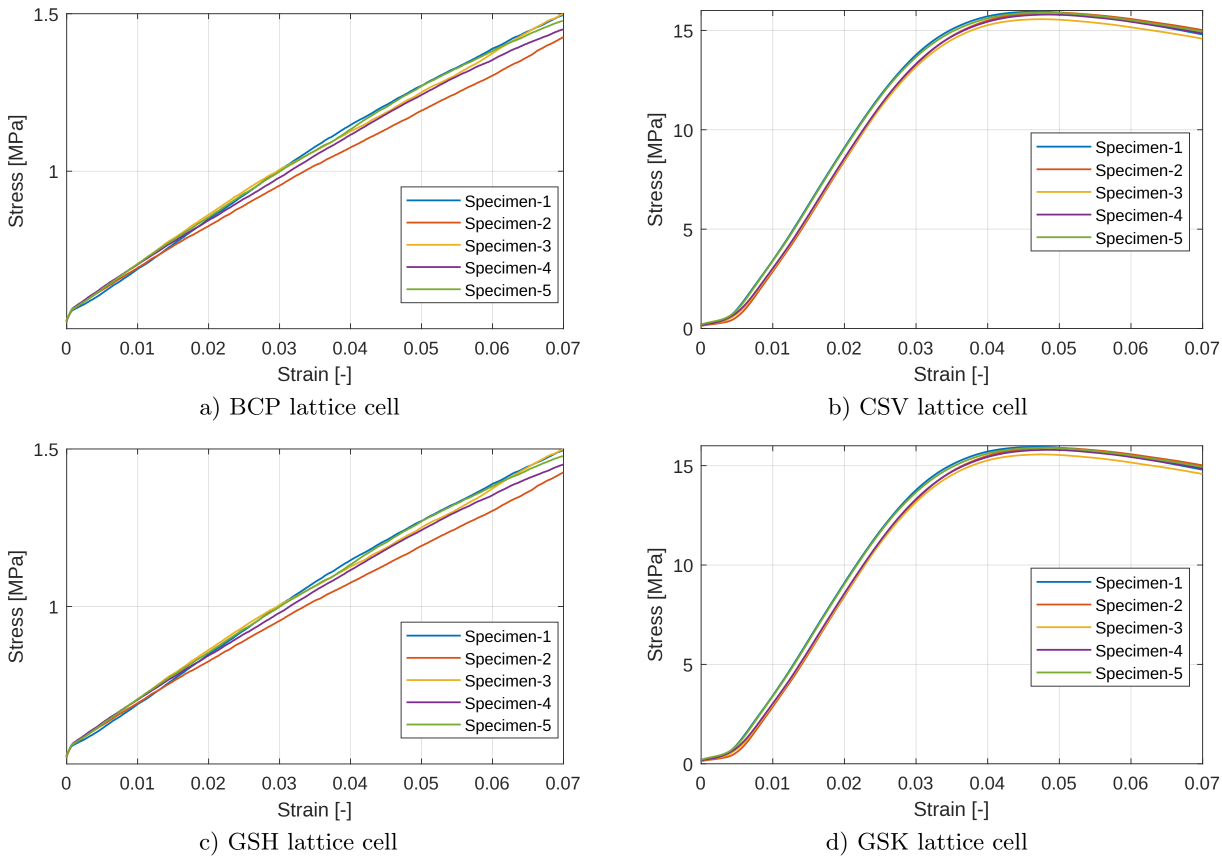

a) BCP lattice cell

b) CSV lattice cell

c) GSH lattice cell

d) GSK lattice cell

Fig. 11. Results of experimental stress-strain curves of lattice cells

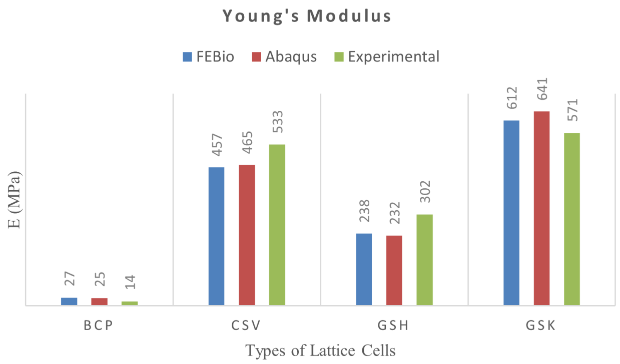

Fig. 12. Young's Modulus results of lattice cells specimens

Discussion

The main aim of this study was to design author lattice cells and identify their mechanical properties by performing numerical analysis and experimental testing. In the scope of this preliminary study, we focused on the uniaxial compression test, since our inspiration was to create lattice structures that imitate bone tissue subjected to compression loading in the linear elastic range of material behavior. Porous structures of proposed lattice cells allow diminishing an occurrence of stress shielding phenomenon, which is a primary cause of implant malfunctioning and influences bone-implant longevity. Furthermore, we assessed Young's moduli of the proposed lattice cells from their numerical results and experimental data. It is worth noting that in clinical practice Young's modulus can be used to match mechanical properties of porous implant (lattice structure) with the bone tissue to ensure proper load distribution in bone-implant system.

In this paper, we described two types of novel lattice cells: regular shapes (BCP and CSV lattice cells) and triply periodic minimal surfaces (GSH and GSK lattice cells). It is worth emphasizing that a design of presented lattice units had to meet a main requirement that involved manufacturing of proposed lattice cells without employing any supporting materials by using the FDM method. That is why a design was based on the iteration approach aiming to find a trade-off between technological limitations of FDM printers (Zortrax and Bambu Lab A1) and developed geometrical models of lattice cells with their numerical models.

Considering results presented in Table 5, we found that the largest relative error of Young's Modulus, which were assessed from experimental data and numerical analysis, is for the BCP lattice unit (47.26% with respect to FEBio and 45.23% with respect to Abaqus). We presume that the cause of this is a very low relative density of this strut-based lattice cell (8.77%) and inner imperfections that could not be identified by visual inspection in the BCP printed samples and might influence the experimental result of Young's Modulus. Moreover, structural integrity of strut-based architectures (BCP) is highly dependent on the FDM staircase effect and nodal junctions (where multiple struts are joined together). These junctions often suffer from localized heat accumulation and material blobbing, which alters the ideal geometry of nodes in the FDM process. Unlike the continuous and smooth curvatures of TPMS structures (CSV, GSH, GSK), the BCP lattice cell transfers load though slender members that are highly sensitive to staircase effects and slight axial misalignments that both are caused by inherent to the layer-by-layer deposition in FDM process. Furthermore, the BCP cell exhibits a bending-dominated deformation mechanism. Consequently, even a slight deviation in BCP strut thickness can lead to a disproportionately large discrepancy between numerically assessed and experimentally calculated results of effective Young's modulus.

Analyzing results of the second regular shape (CSV lattice cell), we identified that a relative error of Young's Modulus of this cell equaled 16.65% with respect to FEBio and 14.64% with respect to Abaqus. This lattice cell is a surface-based unit with a relative density equaling 30.27%, which is three and a half times more than the density of the BCP lattice cell. We can argue that this higher relative density caused the smaller relative error of the CSV lattice cell with respect to the BCP lattice cell.

Considering two TPMS lattice cells GSH and GSK, we found that relative errors of Young's Modulus of the GSH lattice cell are higher (30.40% with respect to FEBio and 30.40% with respect to Abaqus) in comparison to the GSK lattice cell (6.60% with respect to FEBio and 10.91% with respect to Abaqus). We can presume that the cause of this difference is different relative densities of these two surface-based units, i.e., 32.31% for the GSH lattice cell and 66.17% for the GSK lattice cell.

Considering relative errors results, we can see the following ranking from the highest to the lowest relative errors: BCP (8.77%), GSH (32.31%), CSV (30.27%), GSK (66.17%). The reason of this could be explained by the nature of 3D printing (new layers are created through adding next filament layer to the previous ones along with the FDM staircase effects), the way of compressing loading transition that is depended on the topology of proposed lattice cells, and implementation of isotropic material model that assumes isotropic mechanical properties.

In addition, one may argue that the cause of the presented relative errors is different filaments used to produce lattice cells: CSV and GSK (Bambu ABS filament), BCP and GSH (Z-ABS filament). Perhaps the quality of the filament also can be treated as an important factor that influence homogeneity and mechanical properties of lattice structures printed by using the Bambu ABS filament (low relative errors) with respect to the lattice structures produced by using the Z-ABS filament (high relative errors).

Comparing results of Young's Modulus obtained from both FEBio and Abaqus, we can see that they are closely related to each other with a correlation coefficient (r) of 99.95%. This shows that both FEM packages can be used to model complex lattice structures in the linear elastic range of material behavior.

Analyzing results of Young's Modulus, we can identify the following order related to resistance of elastic deformation of the tested lattice cells:1) BCP unit (14.24 MPa (experimental) vs 27.00/25.00 MPa (numerical)); 2) GSH unit (302.08 MPa (experimental) vs 238.22/231.54 MPa (numerical)); 3) CSV unit (532.97 MPa (experimental) vs 456.90/464.92 MPa (numerical)); 4) GSK unit (571.33 MPa (experimental) vs 611.69/641.27 MPa (numerical)). Comparing these results with the published ones, it was concluded that our results are new ones. For example, in Wojnicz et al. (2021) there are described experimental results of effective Young's moduli assessed from uniaxial compression of lattice structures: 1) the lowest value was obtained for the rhombic dodecahedron structure (52.3MPa), lattice octahedron structure (59.3MPa) and truncated octahedron structure (60.8MPa); 2) the highest value was estimated for the regular cubic structure (117.6 MPa) and subtractive structure (114.2MPa). Furthermore, the paper Chatzigeorgiou et al. (2022) describes the TPMS structures and presents results of normalized effective Young's modulus that cannot be directly compared to our results due to this normalized presentation. Moreover, the paper Leite et al. (2018) presents results of Young's modulus estimated for untreated ABS samples produced by the FDM method with different raster angles. Loading these samples by uniaxial loading, the authors obtained: 742.1 MPa (90 raster angle) and 800.3MPa (45 raster angle). It is worth paying attention that these raster angles (printing directions) should be treated as a very important factor that influences mechanical properties of the tested ABS samples (Quan et al., 2018). Also, the paper Mishra et al. (2021) presents results of experimental testing of the Schwarz-P surface produced by the FDM method from the ABS filament: the average of Young's Modulus is equaled 106.63 MPa for 5 mm/min uniaxial compressive loading. Moreover, the paper Yu et al. (2019) describes results of Young modulus estimated for the Schwarz P and Gyroid structures (with a wall thickness up to 2.10 mm) that were uniaxially compressed in the printed direction: uniform Schwarz P (60.07 MPa) and graded Schwarz P (59.76 MPa), uniform gyroid (41.06 MPa) and graded gyroid (49.36 MPa). It is worth emphasizing that Young's modulus of a tested lattice structure is also dependent on the technological factors of the used 3D printer. That is why a selection of optimized parameters should be done in the preliminary step by applying the trials-and-errors method (Lay et al., 2019).

A comparative mechanistic analysis in the liner-elastic range of material behavior reveals significant differences in the load-transmission paths of the four lattice architectures. The BCP lattice cell exhibited a bending-dominated response, which was mainly caused by a lower nodal connectivity (where a structural integrity of each BCP strut is governed by the flexural rigidity). Subsequently, the largest deformation occurring in the nodal junction increased the risk of premature localized failure. On the other hand, tested TPMS structures exhibited surface-distributed load transition, which depended on the curvatures of TPMS walls, and could be treated as a stretch-dominated mechanism. TPMS structures' mechanistic behavior under compressive loading can be assessed as a more stable with respect to the tested BCP structure. Considering numerical and experimental results of Young's moduli of lattice cells tested in this study, we can conclude that surface-based lattice cells (CSV, GSH, GSK) are less sensitive to the slight FDM imperfections, which are caused by the FDM process, than a strut-based lattice cell (BCP). From a scientific perspective our findings show that TPMS lattice cells can be treated as more reliable candidates for patient-specific implants, as their mechanical properties are less sensitive to deterioration caused by micro-scale imperfections occurred in the FDM printed objects.

Overall dimensions of numerical models of proposed lattice cells were selected to be close to each other. On the other hand, overall dimensions of experimental specimens were a little bit higher with respect to the dimensions of numerical models. The reason for these differences was caused by the requirement to produce an accurate geometrical shape by using two 3D printers with a 0.4 mm diameter nozzle.

In this study, we implemented an isotropic material model that allows us to assess mechanical properties of proposed lattice cells in compressive static test by calculating Youngs' moduli (results are presented in Table 5). It is worth noticing that Young's modulus result, which is not dependent on the size of the sample, also considers influence of cross-section area and length of tested specimen/model while coefficient of stiffness is a relation between load (normal force) and change in length along the line of acting of this load.

The limitations of this study are as follows. First, two 3D printers (Zortrax M200 and Bambu Lab A1) used in this study introduced slight geometric deviations with respect to the idealized CAD models. These variations occurred in wall thickness, and surface roughness might influence the mechanical properties of printed lattice cells. Second, numerical analysis had been conducted in the linear elastic regime using available computational capacity. For each of the lattice cell numerical models, we performed numerical analysis with different mesh sizes and chose an optimum mesh size that allowed us to obtain numerically converged results.

Conclusion

In this paper we present a methodological validation of numerical models, that were created in an open-source software (FEBio) and commercial one (Abaqus), against experimental results obtained from mechanical testing of specimens manufactured by using FDM technology. In our study, we produced four types of lattice cells by applying an approach based on a closed iteration procedure involving four steps: 1) geometrical design; 2) numerical analysis; 3) manufacturing (technological problems); 4) experimental testing. A manufacturing of each lattice cell demanded to satisfy two main requirements: 1) each cell has to be produced by using FDM technique without any supports; 2) overall dimensions of each cell should be as small as possible to produce accurate geometrical shape that is limited by technical possibilities of 3D FDM printers used in this study.

Comparing numerical results with experimental ones, we can state that presented results indicate suitability for broader applications in biomedical and mechanical research. While highly complex constitutive models are often necessary for capturing the full response of tested lattice cells, the very first step in establishing numerical model trustworthiness is verifying accuracy by considering a linear-elastic range of material behavior. Moreover, one should remember that mechanical properties of 3D printed lattice structures are dependent on the technological factors of the used FDM printer. Furthermore, the same type of material can have a bit different mechanical properties in different FDM technology, e.g. ABS filament used in Bambu Lab A1 printer (Bambu ABS) and in Zortrax (Z ABS), i.e. ABS filament.

While FEBio is zero cost and with specialized features for biomaterials, Abaqus is a professional software with multidiscipline applications. However, both software can give nearly the same numerical results (*correlation coefficient* of 99.95%) for complex lattice cells in a linear elastic-range of material models loaded by static uniaxial compression. With respect to time, the total computational time used by Abaqus (80 minutes) is four times that of FEBio (20 minutes) for all the models.

To design lattice cells with a demanded mechanical property, one can degrade the Young's modulus of a solid member by imposing porosity. However, the geometry of this porosity distribution influences the mechanical properties of this porous member. For example, the CSV and GSH lattice cells are characterized by the close relative density, but their Young's moduli are quite different.

It is worth noticing that lattice cells described in this study should be treated as porous structures that are the fundamental structures of a trabecular bone tissue. Empty space between porous structures can be filled with different media. However, an extended study should be conducted to identify the interaction phenomena between tested porous structure and this media.

This study goes beyond a preliminary comparative analysis of lattice geometries by proposing the following two implications to the field of additive manufacturing and biomechanical engineering. First, we propose a benchmarked validation of two software (open-source software (FEBio) and commercial one (Abaqus)) that were used to analyze complex lattice cells (TPMS and strut-based geometries) in the linear-elastic range of material behavior. Obtained findings indicate that used software can be treated as a validated and accessible workflow for researchers to predict the modulus of elasticity of bio-mimetic scaffolds without the need for usage of proprietary software. Second, we revealed that lattice topology influences an error margin of FDM specimens. Specifically, the analysis shows that BCP geometries exhibit higher sensitivity to FDM-induced nodal imperfections compared to TPMS-based lattices. This provides a quantitative basis for selecting printable architectures that are characterized by designed mechanical properties despite inherent limitations of 3D printing technology based on a polymer deposition.

Aiming to explore the nature of presented discrepancy (relative errors) our future study involves considering: 1) implementation of non-linear constitutive model (also orthotropic) to analyze non-linear mechanical behavior and failure mechanisms of proposed lattice cells and their assemblies; 2) optimization of topology of proposed lattice cells; 3) numerical and experimental testing of structural integrity of proposed lattice cells (and their assemblies) subjected to the complex static loading, fatigue and dynamic loading along with an identification of factors that may provide instabilities (e.g. buckling) and initiate damage process.

Acknowledgements

The calculations were carried out at the Academic computer Centre in Gdansk (TASK), Poland.

References

Ali, S., Deiab, I., Pervaiz, S., (2024). State-of-the-art review on fused deposition modeling (FDM) for 3D printing of polymer blends and composites: innovations, challenges, and applications," *Int. J. Adv. Manuf. Technol.*, *135*(11), 5085–5113, Dec. 2024, DOI: 10.1007/s00170-024-14820-0

Al-Ketan, O., Lee, D.W., Rowshan, R., Abu Al-Rub, R.K., (2020). Functionally graded and multi-morphology sheet TPMS lattices: Design, manufacturing, and mechanical properties, *J. Mech. Behav. Biomed. Mater.*, *102*, 103520, DOI: 10.1016/j.jmbbm.2019.103520

Ansari, A.I., Sheikh, N.A., Kumar, N., (2024). "Evaluation of the energy absorbing capacity of the two combinations of TPMS structure subjected to different compressive strain rates," *J. Braz. Soc. Mech. Sci. Eng.*, *46*(6), 334, May 2024, DOI: 10.1007/s40430-024-04925-8

Chatzigeorgiou, C., Piotrowski, B., Chemisky, Y., Laheurte, P., Meraghni, F., (2022). "Numerical investigation of the effective mechanical properties and local stress distributions of TPMS-based and strut-based lattices for biomedical applications," *J. Mech. Behav. Biomed. Mater.*, *126*, 105025, Feb. 2022, DOI: 10.1016/j.jmbbm.2021.105025

Chibinyani, M.I., Dzogbewu, T.C., Maringa, M., Muiruri, A., (2025). Natural cellular structures in engineering designs built via additive manufacturing," *Mater. Technol.*, Dec. 2025, DOI: 10.1080/10667857.2024.2443211

Dimitrellou, S., Strantzali, E., Iakovidis, I., (2025). A decision-making strategy for selection of FDM-based additively manufactured thermoplastics for industrial applications based on material attributes," *Sustain. Futur.*, *9*, 100640, Jun. 2025, DOI: 10.1016/j.sftr.2025.100640

Dong, G., Tang, Y., Zhao, Y.F., (2017). A Survey of Modeling of Lattice Structures Fabricated by Additive Manufacturing," *J. Mech. Des.*, *139*(100906), Aug. 2017, DOI: 10.1115/1.4037305

Dong, G., Tang, Y., Li, D., Zhao, Y.F., (2020). Design and optimization of solid lattice hybrid structures fabricated by additive manufacturing," *Addit. Manuf.*, *33*, 101116, May 2020, DOI: 10.1016/j.addma.2020.101116

Evans, A.G., He, M.Y., Deshpande, V.S., Hutchinson, J.W., Jacobsen, A.J., Carter, W.B., (2010) Concepts for enhanced energy absorption using hollow microlattices," *Int. J. Impact Eng.*, *37*(9), 947–959, Sep. 2010, DOI: 10.1016/j.ijimpeng.2010.03.007

Fang, G., Zhang, T., Zhong, S., Chen, X., Zhong, Z., Wang, C.C.L., (2020). Reinforced FDM: multi-axis filament alignment with controlled anisotropic strength," *ACM Trans Graph*, *39*(6), 204:1-204:15, Nov. 2020, DOI: 10.1145/3414685.3417834

Fassi, H.F., Aniyou, H., (2023). Towards an Optimal Motor Mounting Bracket Using Topology Optimization Combined with Sustainability and Manufacturing Cost Analysis," *Manag. Prod. Eng. Rev.*, *14*(4), 2023, DOI: 10.24425/mper.2023.147208

Garzon-Hernandez, S., Garcia-Gonzalez, D., Jérusalem, A., Arias, A., (2020). Design of FDM 3D printed polymers: An experimental-modelling methodology for the prediction of mechanical properties," *Mater. Des.*, *188*, 108414, Mar. 2020, DOI: 10.1016/j.matdes.2019.108414

Geraets, W.G.M., van Ruijven, L.J., Verheij, J.G.C., van der Stelt, P.F., van Eijden, T.M.G.J., (2008). "Spatial orientation in bone samples and Young's modulus," *J. Biomech.*, *41*(10), 2206–2210, Jul. 2008, DOI: 10.1016/j.jbiomech.2008.04.016

Giannitelli, M.M., Accoto, D., Trombetta, M., Rainer, A., (2014). Current trends in the design of scaffolds for computer-aided tissue engineering," *Acta Biomater.*, *10*(2), 580–594, Feb. 2014, DOI: 10.1016/j.actbio.2013.10.024

Gibson, L.J., (2003). Cellular Solids, *MRS Bull.*, *28*(4), 270–274, DOI: 10.1557/mrs2003.79

Gibson, I.J., Ashby, M.F., (1982). The mechanics of three-dimensional cellular materials. *Proc. R. Soc. Lond. Math. Phys. Sci.*, *382*(1782), 43–59, DOI: 10.1098/rspa.1982.0088

Gibson, L.J., Ashby, M.F., (1997). Introduction, in *Cellular Solids: Structure and Properties*, 2nd ed., in Cambridge Solid State Science Series. Cambridge: Cambridge University Press, 1–14. DOI: 10.1017/CBO9781139878326.003

Gurtner, G., Durand, M., (2014). Stiffest elastic networks," *Proc. R. Soc. Math. Phys. Eng. Sci.*, *470*(2164), 20130611, Apr. 2014, DOI: 10.1098/rspa.2013.0611

Han, Y., Lu, W.F., (2018). A Novel Design Method for Nonuniform Lattice Structures Based on Topology Optimization," *J. Mech. Des.*, *140*(091403), Jul. 2018, DOI: 10.1115/1.4040546

Haque, M.M.M. *et al.*, (2025). Impact of process parameters and material selection on the mechanical performance of FDM 3D-Printed components," *Hybrid Adv.*, *10*, 100502, Sep. 2025, DOI: 10.1016/j.hybadv.2025.100502

Hutmacher, D.W., (2000). Scaffolds in tissue engineering bone and cartilage.," *Biomaterials*, *21*(24), 2529–2543, Dec. 2000, DOI: 10.1016/S0142-9612(00)00121-6

Kamal-k-s, *Kamal-k-s/Lattice*. (2025). MATLAB. Accessed: Nov. 07, 2025. [Online]. Available: https://github.com

Karageorgiou, V., Kaplan, D., (2005). Porosity of 3D biomaterial scaffolds and osteogenesis," *Biomaterials*, *26*(27), 5474–5491, Sep. 2005, DOI: 10.1016/j.biomaterials.2005.02.002

Kaur, G., Singari, R.M., Kumar, H., (2022). A review of fused filament fabrication (FFF): Process parameters and their impact on the tribological behavior of polymers (ABS)," *Mater. Today Proc.*, *51*, 854–860, Jan. 2022, DOI: 10.1016/j.matpr.2021.06.274

Lay, M., Thajudin, N.L.N., Hamid, Z.A.A., Rusli, A., Abdullah, M.K., Shuib, R.K., (2019). Comparison of physical and mechanical properties of PLA, ABS and nylon 6 fabricated using fused deposition modeling and injection molding," *Compos. Part B Eng.*, *176*, 107341, Nov. 2019, DOI: 10.1016/j.compositesb.2019.107341

Leite, M., Varanda, A., Ribeiro, A.R., Silva, A., Vaz, M.F., (2018). Mechanical properties and water absorption of surface modified ABS 3D printed by fused deposition modelling," *Rapid Prototyp. J.*, *24*(1), 195–203, Jan. 2018, DOI: 10.1108/RPJ-04-2016-0057

Li, Z., Li, S., Liu, J., Liu, Z., Lei, J., Wang, Z., (2025). Response mechanisms and energy absorption properties of hybrid sheet TPMS lattices under static and dynamic loading," *Thin-Walled Struct.*, *210*, 112980, May 2025, DOI: 10.1016/j.tws.2025.112980

Mahmud, M.S. *et al.*, (2024). Design and evaluation of selective laser sintering of thermoset lattice structures," *Prog. Addit. Manuf.*, Aug. 2024, DOI: 10.1007/s40964-024-00747-1

Mishra, A.K., Kumar, A., (2023). Compression Behavior of Triply Periodic Minimal Surface Polymer Lattice Structures," *Exp. Mech.*, *63*(4), 609–620, Apr. 2023, DOI: 10.1007/s11340-023-00940-3

Mishra, A.K., Chavan, H., Kumar, A., (2021). Effect of material variation on the uniaxial compression behavior of FDM manufactured polymeric TPMS lattice materials," *Mater. Today Proc.*, *46*, 7752–7759, Jan. 2021, DOI: 10.1016/j.matpr.2021.02.276

Narita, M., Citrin, A., Yang, H., Xia, X., Greer, J.R., (2021). 3D Architected Carbon Electrodes for Energy Storage," *Adv. Energy Mater.*, *11*(5), 2002637, 2021, DOI: 10.1002/aenm.202002637

Pan, C., Han, Y., Lu, J., (2020). Design and Optimization of Lattice Structures: A Review," *Appl. Sci.*, *10*(18), 6374, Jan. 2020, DOI: 10.3390/app10186374

Prochor, P., Frossard, L., Sajewicz, E., (2020). Effect of the material's stiffness on stress-shielding in osseointegrated implants for bone-anchored prostheses: a numerical analysis and initial benchmark data," *Acta Bioeng. Biomech.*, *22*(2), 69–81, 2020, DOI: 10.37190/ABB-01543-2020-02

Qi, D., Lu, Q., He, Y., Li, Y., Wu, W., Xiao, D., (2019). Impact energy absorption of functionally graded chiral honeycomb structures," *Extreme Mech. Lett.*, *32*, 100568, Oct. 2019, DOI: 10.1016/j.eml.2019.100568

Quan, Z. *et al.*, (2018). Printing direction dependence of mechanical behavior of additively manufactured 3D preforms and composites," *Compos. Struct.*, *184*, 917–923, Jan. 2018, DOI: 10.1016/j.compstruct.2017.10.055

Shi, L.K., Li, P.C., Liu, C.R., Zhu, J.X., Zhang, T.H., Xiong, G., (2024). An improved tensile strength and failure mode prediction model of FDM 3D printing PLA material: Theoretical and experimental investigations," *J. Build. Eng.*, *90*, 109389, Aug. 2024, DOI: 10.1016/j.jobe.2024.109389

Stampfl, J., Pettermann, H.E., Liska, R., (2011). Bioinspired Cellular Structures: Additive Manufacturing and Mechanical Properties," Berlin, Heidelberg: Springer, 2011, 105–123. DOI: 10.1007/978-3-642-11934-7_6

Stanković, T., Mueller, J., Egan, P., Shea, K., (2015). A Generalized Optimality Criteria Method for Optimization of Additively Manufactured Multimaterial Lattice Structures," *J. Mech. Des.*, *137*(111405), Oct. 2015, DOI: 10.1115/1.4030995

Stanković, T., Mueller, J., Shea, K., (2017). The effect of anisotropy on the optimization of additively manufactured lattice structures," *Addit. Manuf.*, *17*, 67–76, Oct. 2017, DOI: 10.1016/j.addma.2017.07.004

Sun, Y. *et al.*, (2025). Understanding the relationship between pore structure and properties of triply periodic minimal surface bone scaffolds," *J. Mater. Sci. Mater. Med.*, *36*(1), 6, Dec. 2025, DOI: 10.1007/s10856-024-06856-1

Szemeti, G., Ramanujan, D., (2022). An Empirical Benchmark for Resource Use in Fused Deposition Modelling 3D Printing of Isovolumetric Mechanical Components," *Procedia CIRP*, *105*, 183–191, Jan. 2022, DOI: 10.1016/j.procir.2022.02.030

Tang, Y., Zhao, Y.F., (2016). A survey of the design methods for additive manufacturing to improve functional performance," *Rapid Prototyp. J.*, *22*(3), 569–590, Apr. 2016, DOI: 10.1108/RPJ-01-2015-0011

Tang, Y., Lin, J., Ye, J., Wei, T., Chen, P., Xu, M., (2025). Analysis of Mechanical Properties of Hybrid Lattice Structures Based on Complementary Elastic Modulus Strategy," *Int. J. Precis. Eng. Manuf.*, *26*(8), 2053–2071, Aug. 2025, DOI: 10.1007/s12541-025-01239-0

Theriot, E., Herbarium, D., (1992). Review of The Diatoms. Biology and Morphology of the Genera. *Syst. Biol.*, *41*(efeq1), 125–126, 1992, DOI: 10.2307/2992511

Wadley, H.N.G., (2005). Multifunctional periodic cellular metals," *Philos. Trans. R. Soc. Math. Phys. Eng. Sci.*, *364*(1838), 31–68, Dec. 2005, DOI: 10.1098/rsta.2005.1697

Wojnicz, W., Augustyniak, M., Borzyszkowski, P., (2021). Mathematical approach to design 3D scaffolds for the 3D printable bone implant," *Biocybern. Biomed. Eng.*, *41*(2), 667–678, Apr. 2021, DOI: 10.1016/j.bbe.2021.05.001

Xu, S., Huang, X., Xie, Y.M., Shen, J., Zhou, S., (2016). Design of lattice structures with controlled anisotropy," *Mater. Des.*, *93*, 443–447, Mar. 2016, DOI: 10.1016/j.matdes.2016.01.007

Yang, L., Cormier, D., West, H., Harrysson, O., Knowlson, K., (2012). Non-stochastic Ti–6Al–4V foam structures with negative Poisson's ratio," *Mater. Sci. Eng. A*, *558*, 579–585, Dec. 2012, DOI: 10.1016/j.msea.2012.08.053

Yang, X.Y., Huang, X., Rong, J.H., Xie, Y.M., (2013). Design of 3D orthotropic materials with prescribed ratios for effective Young's moduli," *Comput. Mater. Sci.*, *67*, 229–237, Feb. 2013, DOI: 10.1016/j.commatsci.2012.08.043

Yu, S., Sun, J., Bai, J., (2019). Investigation of functionally graded TPMS structures fabricated by additive manufacturing," *Mater. Des.*, *182*, 108021, Nov. 2019, DOI: 10.1016/j.matdes.2019.108021